Progress In Electromagnetics Research, PIER 76, 449–466, 2007

PROPAGATION PROPERTIES OF THE SPP MODES IN NANOSCALE NARROW METALLIC GAP, CHANNEL, AND HOLE GEOMETRIES

F. M. Kong and K. Li

School of Information Science and Engineering
Shandong University
Jinan, 250100, P. R. China

B. I. Wu

Research Laboratory of Electronics
Massachusetts Institute of Technology
Cambridge, MA 02139, USA

H. Huang

School of Electrical Engineering
Beijing Jiaotong University
Beijing, 100044, P. R. China

H. S. Chen

The Electromagnetics Academy at Zhejiang University
Zhejiang University
Hangzhou, 310058, P. R. China

J. A. Kong

Research Laboratory of Electronics
Massachusetts Institute of Technology
Cambridge, MA 02139, USA

Abstract—The propagation properties of surface plasmon polaritons (SPP) modes in nanoscale narrow metallic structures: gap, channel, and rectangular-hole waveguides, are analyzed by the complex effective dielectric constant approximation. The results show that all the SPP modes exist below the critical frequency where the real part of metal permittivity is negative unity. It is found that both cutoff frequency and cutoff height exist in channel waveguide and rectangular-hole waveguide. The channel and rectangular-hole waveguides have different propagation properties at cutoffs due to their different cutoff conditions. Compared with the gap waveguide, the channel waveguide has shorter propagation length and better confinement when the operation frequency is near the critical frequency, but has longer propagation length and worse confinement when the operation frequency is far from the critical frequency. Among the three waveguides, the rectangular-hole waveguide has the best confinement factor and the shortest propagation length. The comprehensive analysis for the gap, channel, and rectangular-hole waveguides can provide some guidelines in the design of subwavelength optical devices.

1. INTRODUCTION

The surface plasmon polaritons (SPP) [1] on a metal-dielectric interface offered a new route to nanophotonics [2, 3]. Phenomena such as enhanced light transmission and light confinement have been found in subwavelength metallic structures [4–8]. The extensive studies of SPPs were not only focused in the challenging of diffraction limit, but also in related potential nanophotonic application in near-field optical microscopy [9], optical data storage [10], nano-lithography [11], and bio-photonics [12].

In order to guide and confine the SPP in highly integrated photonic circuits, various plasmonic waveguides have been introduced, such as metallic photonic crystals [13], thin metal strip [14], metal nanoparticle chains [15, 16], metal nanorods [17], and V-groove[18-20]. Among these plasmonic waveguide structures, long-range SPP waveguide based on thin metal stripe has been intensively investigated both theoretically and experimentally [21–23]. However, since the localization in both transverse directions of this geometry is on the order of a few micrometers, it does not have good potential for applications in high photonic integration. So far, the V-groove, which is characterized by strong localization, relatively low dissipation, single mode operation, low loss, and high tolerance to structural imperfections, seems to be one of the best options for subwavelength

guiding. Recently, some highly localized plasmonic waveguides, for example, nanoscale metallic gap [24, 25], channel [26, 27], and rectangular-hole structures [5, 28], which are similar to metallic stripe line, slot line, and rectangular waveguide in microwave frequencies, have been proposed to guide and confine SPP modes in the optical frequencies. It is expected that such plasmonic waveguides will become a basic building block of future integrated nanophotonic devices with spatial dimensions below the diffraction limit.

In optical frequencies, the properties of the metals can generally be described by complex permittivity with dispersion and loss. Furthermore, the real part of metal permittivity can be negative below the plasma frequency. Thus, the metal is greatly different from perfect conductor in microwave frequencies, and some analytic solutions and approximations which have been used in microwave frequencies are not valid for analyzing the metallic structures in optical frequencies. Also, the SPP confinement in metallic structure is achieved by decreasing the SPP spatial extent into dielectric, thereby increasing the portion of SPP power being absorbed by metal; hence the optimum configuration of plasmonic structure is subjected to many intricate issues. In order to analyze the light transmission through subwavelength metallic structures, finite-difference methods in time domain and frequency domain have been used to study the guided modes and transmission characteristics in plasmonic waveguides [29, 30]. Due to the large discrepancy of permittivities between metal and dielectric, finite-difference method may cause calculation instability when applied to certain nanoscale metallic structures. Recently, the effective dielectric constant method, which is one of the standard approaches used for lossless waveguide analysis in photonics [31], has been used to analyze the fundamental mode in the plasmonic waveguide [32] and the results are in good quantitative agreement with other numerical methods.

In this paper, the complex dielectric constant method is used to analyze the SPP modes in the narrow lossy metallic waveguide where the permittivity of the metal is represented by the Drude model. Three typical metallic geometries: gap, channel, and rectangular-hole waveguides are analyzed by calculating the mode effective index, propagation length, confinement factor, and beam diameter from 200 THz to the critical frequency. The height dependence of the SPP modes in the gap, channel, and rectangular-hole waveguides is presented and the field distributions in those waveguides are studied for different wavelengths. Finally, the propagation properties of the gap, channel, and rectangular-hole waveguides are analyzed and compared for the same size air-core.

2. ANALYSIS METHODOLOGY

Figure 1 shows three different metallic waveguide structures under consideration: gap, channel, and rectangular-hole structures. In fact, the channel waveguide can be treated as a strong asymmetric gap waveguide with metal substrate and dielectric cladding, and the rectangular-hole waveguide can be considered as a special symmetric waveguide.

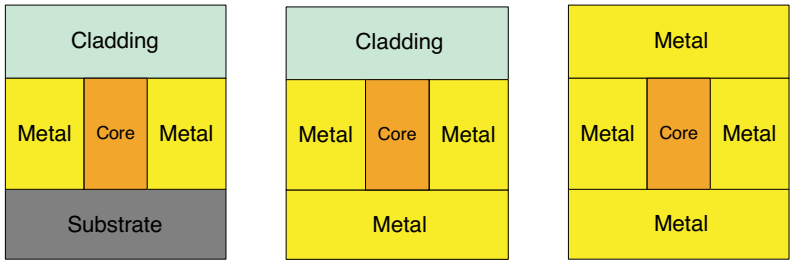

(a) Gap structure (b) Channel structure (c) Hole structure

Figure 1. Configuration of the narrow metallic waveguides.

The relative dielectric constants of the core, cladding, and substrate are assumed to be $\varepsilon_{rf}, \varepsilon_{rc}$, and ε_{rs}. The complex dielectric constant of metal at optical frequencies is approximated by the Drude model as follows:

$$\varepsilon_{rm}(\omega) = \varepsilon_{\infty}\left(1 - \frac{\omega_p^2}{\omega(\omega + i\omega_\tau)}\right) \tag{1}$$

where ε_{∞} is the permittivity at infinite frequency, ω_p and ω_τ are the plasma and collision frequencies respectively.

The concept of the effective dielectric constant approach is shown in Figure 2. The cross section of metallic waveguide (Figure 2(a)) can be treated as a combination of two coupled 1D slab waveguides in the y and x directions respectively (Figures 2(b), (c)).

When the waveguide width w is smaller than the waveguide height h, the primary mode in the narrow waveguide is the x-polarized electric field mode, where E_x and H_y are the principal field components. The wave function for the slab waveguide along y-axis (Figure 2(b)) can be written as [33]:

$$\phi_{H_y}(x) = \begin{cases} B_1 e^{-\gamma_x(x-w/2)} & (x > w/2) \\ A_1 e^{ik_x x} + A_2 e^{-ik_x x} & (-w/2 \le x \le w/2) \\ B_2 e^{+\gamma_x(x+w/2)} & (x < -w/2) \end{cases} \tag{2}$$

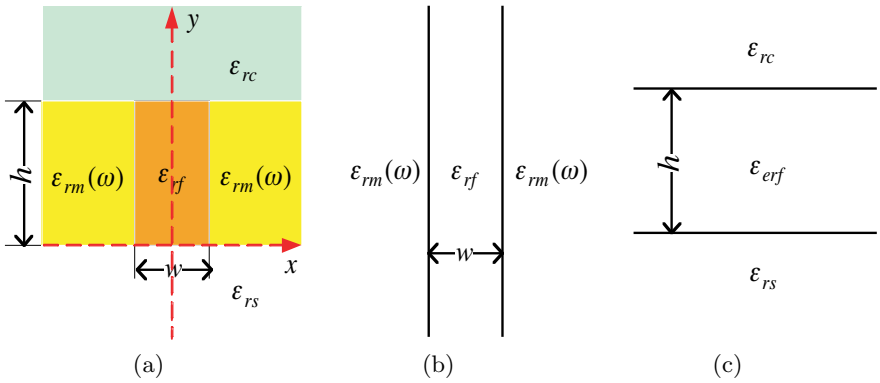

Figure 2. (a) Cross section of metallic waveguide. (b) An equivalent 1-D slab in the y direction. (c) An equivalent 1-D slab in the x direction. ε_{erf} is the effective dielectric constant in the slab.

Applying the boundary conditions at $x = \pm w/2 : E_{z1} = E_{z2}$ and $H_{y1} = H_{y2}$, we get

$$\frac{ik_x}{\varepsilon_{rf}}\left(A_1 e^{\frac{ik_x w}{2}} - A_2 e^{-\frac{ik_x w}{2}}\right) = -\frac{B_1\gamma_x}{\varepsilon_{rm}(\omega)} \tag{3a}$$

$$A_1 e^{\frac{ik_x w}{2}} + A_2 e^{-\frac{ik_x w}{2}} = B_1 \tag{3b}$$

$$\frac{ik_x}{\varepsilon_{rf}}\left(A_1 e^{-\frac{ik_x w}{2}} - A_2 e^{\frac{ik_x w}{2}}\right) = \frac{B_2\gamma_x}{\varepsilon_{rm}(\omega)} \tag{3c}$$

$$A_1 e^{-\frac{ik_x w}{2}} + A_2 e^{\frac{ik_x w}{2}} = B_2 \tag{3d}$$

Eliminating the constants in Eq. (3), we obtain the guidance condition for the y-axis slab waveguide

$$\tan(k_x w) = \frac{2\rho_x}{1-\rho_x^2} \tag{4}$$

where $\rho_x = \frac{\varepsilon_{rf}\gamma_x}{\varepsilon_{rm}(\omega)k_x}$ and $\gamma_x^2 = k_0^2(\varepsilon_{rf} - \varepsilon_{rm}(\omega)) - k_x^2$.

The effective dielectric constant for the y-axis slab waveguide can be expressed as

$$\varepsilon_{erf} = \varepsilon_{rf} - (k_x/k_0)^2 \tag{5}$$

Thus, the metallic waveguide can be regarded as a lossy slab waveguide along x-axis with the complex effective dielectric constant ε_{erf} in the core (Figure 2(c)), and the wave functions for the x-axis slab waveguide

can be expressed as

$$\phi_{E_x}(y) = \begin{cases} D_1 e^{-\gamma_{cy}(y-h)} & (y > h) \\ C_1 e^{ik_y y} + C_2 e^{-ik_y y} & (0 \le y \le h) \\ D_2 e^{\gamma_{sy} y} & (y < 0) \end{cases} \tag{6}$$

Applying the boundary conditions at $y = 0, h$: $H_{z1} = H_{z2}$ and $E_{x1} = E_{x2}$, we get

$$ik_y(C_1 - C_2) = D_2\gamma_{sy} \tag{7a}$$
$$C_1 + C_2 = D_2 \tag{7b}$$
$$ik_y\left(C_1 e^{ik_y h} - C_2 e^{-ik_y h}\right) = -D_1\gamma_{cy} \tag{7c}$$
$$C_1 e^{ik_y h} + C_2 e^{-ik_y h} = D_1 \tag{7d}$$

Eliminating the constants in Eq. (7), we can get the guidance condition for the x-axis slab waveguide

$$\tan(k_y h) = \frac{\rho_{cy} + \rho_{sy}}{1 - \rho_{cy}\rho_{sy}} \tag{8}$$

where $\rho_{cy} = \gamma_{cy}/k_y$, $\rho_{sy} = \gamma_{sy}/k_y$, $\gamma_{cy}^2 = k_0^2(\varepsilon_{erf} - \varepsilon_{rc}) - k_y^2$ and $\gamma_{sy}^2 = k_0^2(\varepsilon_{erf} - \varepsilon_{rs}) - k_y^2$.

It should be pointed out that the transverse parameters γ_x, γ_{cy}, and γ_{sy}, which indicate the radiation from the metallic waveguide, may be complex, and the condition that Re $(\gamma_x) > 0$, Re$(\gamma_{cy}) > 0$, and Re$(\gamma_{sy}) > 0$ are needed to ensure the boundary condition at infinity.

To solve k_x and k_y numerically, Eq. (4) and Eq. (8) can be written in a convenient form as

$$k_x w = 2\arctan(\rho_x) + (m-1)\pi \qquad (m = 1, 2) \tag{9}$$
$$k_y h = \arctan(\rho_{cy}) + \arctan(\rho_{sy}) + (n-1)\pi \quad (n = 1, 2, \ldots) \tag{10}$$

and the surface plasmon modes with x-polarized electric fields in the narrow metallic waveguide are denoted as SP_{mn}^x, where the subscripts $m = 1$ and $m = 2$ correspond to the even and odd symmetries of the field distributions in the x direction, and the subscript n is the number of the peak in the field along the y direction.

Determining the precise mode solution of a metallic waveguide involves finding the complex k_x and k_y in the dispersion relations in Eq. (9) and Eq. (10), the complex propagation constant β can be expressed as

$$\beta = \sqrt{k_0^2\varepsilon_{rf} - k_x^2 - k_y^2} \tag{11}$$

where the real part of β is related to the effective index of SPP mode, i.e., $N_{eff} = \mathrm{Re}(\beta)/k_0$, whereas its imaginary part determines the SPP propagation length: $L = (2\mathrm{Im}(\beta))^{-1}$.

The H_y field in the core region and its neighborhoods could be written as

$$H_y(x,y) = \begin{cases} H_0 \cos(k_x x)(\cos(k_y y) + \gamma_{sy}/k_y \sin(k_y y)) \\ \qquad -w/2 \le x \le w/2,\ 0 \le y \le h \\ H_0 \cos(k_x w/2) e^{-\gamma_x (x-w/2)}(\cos(k_y y) + \gamma_{sy}/k_y \sin(k_y y)) \\ \qquad x > w/2,\ 0 < y < h \\ H_0 \cos(k_x w/2) e^{\gamma_x (x+w/2)}(\cos(k_y y) + \gamma_{sy}/k_y \sin(k_y y)) \\ \qquad x < -w/2,\ 0 < y < h \\ H_0 \cos(k_x x)(\cos(k_y h) + \gamma_{sy}/k_y \sin(k_y h)) e^{-\gamma_{cy}(y-h)} \\ \qquad -w/2 < x < w/2,\ y > h \\ H_0 \cos(k_x x) e^{\gamma_{sy} y} \quad -w/2 < x < w/2,\ y < 0 \end{cases} \tag{12}$$

3. RESULTS AND DISCUSSION

In this section, the optical propagation characteristics of narrow metallic gap, channel and rectangular-hole waveguides are studied by using the complex effective dielectric constant method. The parameters $\varepsilon_\infty = 3.7$, $\omega_p = 7.11 \times 10^{15}$ rad/s, and $\omega_\tau = 2.735 \times 10^{13}$ rad/s are chosen to model the permittivity of silver [34]. The permittivity for silver at $\lambda = 632.8$ nm can be obtained by $\varepsilon_{rm} = -17.385 + 0.21i$. According to the parameters above, the critical frequency f_c for the SPP modes existence, where the permittivity for silver is negative unity, is 1003 THz.

In order to quantify the energy confinement in these metallic waveguides, the beam diameter and the confinement factor are defined. The beam diameter describes the spatial extent of propagation mode by the distance between the points where the magnetic field H_y decays to $1/e$ of its peak values. Since the beam diameter in the x-direction is mainly limited by the distance between the two metal films, only the beam diameter in the y-direction is discussed. The confinement factor represents the ratio of power in the core region to the total power in the waveguide and is defined as:

$$F_c = \frac{\int_{-w/2}^{w/2} \int_0^h E_x(x,y) H_y^*(x,y) dx dy}{\int_{-\infty}^{\infty} \int_{-\infty}^{\infty} E_x(x,y) H_y^*(x,y) dx dy} \tag{13}$$

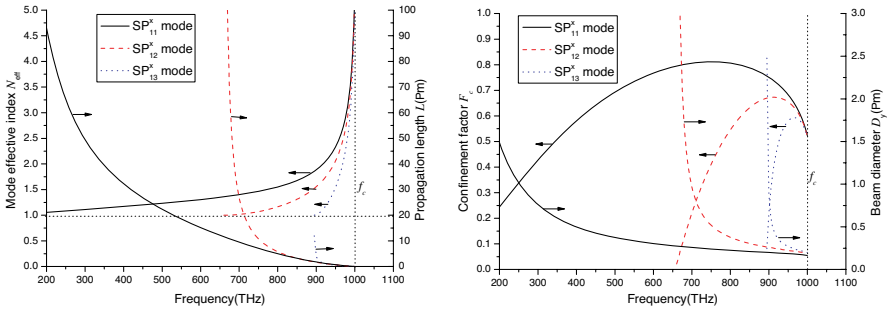

(a) Mode effective index and propagation length (b) Confinement factor and beam diameter

Figure 3. The propagation properties of the SPP modes in gap waveguide as a function of frequency.

3.1. Gap Waveguide

The gap waveguide is one of the useful plasmonic waveguides and has high transmission through sharp bends [35]. For comparison with the channel and hole waveguides, the dielectric constants of the core, cladding and substrate in gap waveguide are assumed to be $\varepsilon_{rf} = \varepsilon_{rc} = \varepsilon_{rs} = 1.0$.

Figure 3 shows the propagation properties of the SPP modes in the gap waveguide with $w = 50\,\text{nm}$ and $h = 200\,\text{nm}$. It is shown that all SPP modes are located in the slow wave regime where mode effective index $N_{eff} > 1$, and the fundamental mode SP^x_{11} does not have cutoff frequency while the higher order modes SP^x_{12} and SP^x_{13} have cutoffs. Compared with SP^x_{12} and SP^x_{13} modes, the SP^x_{11} mode has better confinement factor and slightly shorter propagation length. As the operation frequency increases, the propagation length decreases and the beam diameter in the y-direction also decreases, but the confinement factor does not increase continuously as expected: it first increases, reaches the maximum, and then starts to decrease. Thus, it seems that there is a conflict between the trends of confinement factor and the beam diameter near the critical frequency. In fact, the SPP mode in the gap can be considered as two coupled SPP modes associated with each metal-dielectric interfaces, and when the SPP mode is close to the critical frequency, the coupling between the two SPP modes is so weak that there is a little energy confined in the air-core in spite of the small beam diameter, resulting in a small confinement factor near the critical frequency.

Figure 4 shows the dependence of the propagation properties of the SPP modes on the height of gap waveguide with $w = 50\,\text{nm}$

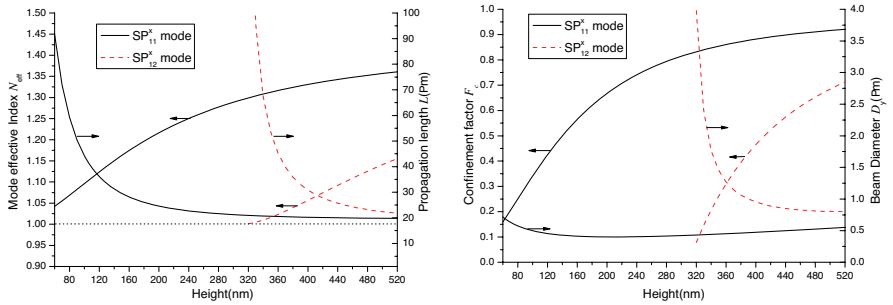

(a) Mode effective index and propagation length (b) Confinement factor and beam diameter

Figure 4. The propagation properties of the SPP modes in gap waveguide as a function of waveguide height.

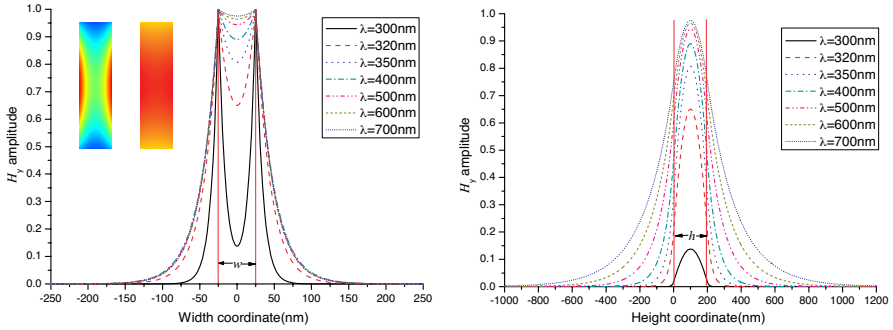

(a) H_y field distribution at y=h/2 (b) H_y field distribution at x=0

Figure 5. The distribution of magnetic field H_y for the fundamental mode SP^x_{11} in the gap waveguide with $w = 50\,\text{nm}$ and $h = 200\,\text{nm}$. The inset shows the H_y field distributions in the air-core at $\lambda = 310\,\text{nm}$ and $632.8\,\text{nm}$ separately.

and $\lambda = 632.8\,\text{nm}$. It is shown that the SPP modes tend to be confined in higher refractive index region and the larger effective indices correspond to smaller propagation lengths and better field confinement factors. Furthermore, the propagation length of the SPP mode starts to increase rapidly when the gap height decreases towards $200\,\text{nm}$, and the effective index approaches that of air-core. The increase of propagation length signifies the tendency of the SPP mode field being extended outside the gap.

Figure 5 shows the distribution of the magnetic field H_y for the SP^x_{11} mode in a gap waveguide with $w = 50\,\text{nm}$ and $h = 200\,\text{nm}$.

As the operation wavelength increases, the delocalization of the two peaks of the SPP mode in the two metal-dielectric interfaces causes more power be concentrated in the air-core of the gap waveguide.

3.2. Channel Waveguide

The channel waveguide is another promising plasmonic waveguide and has exhibited practical subwavelength confinement with moderate propagation loss. The channel waveguide can be treated as a strong asymmetric gap waveguide with silver substrate and air cladding.

Figure 6 shows the propagation properties of the SPP modes in the channel waveguide with $w = 50\,\text{nm}$ and $h = 200\,\text{nm}$. The results show that all SPP modes in the channel waveguide exist below the critical frequency and can be found in the slow wave regime. As the operating frequency decreases from the critical frequency, all the SPP modes will reach cutoff at certain frequencies due to the asymmetry between the substrate and the cladding. Compared with higher order modes SP_{12}^x and SP_{13}^x, the fundamental mode SP_{11}^x has better confinement factor and slightly longer propagation length.

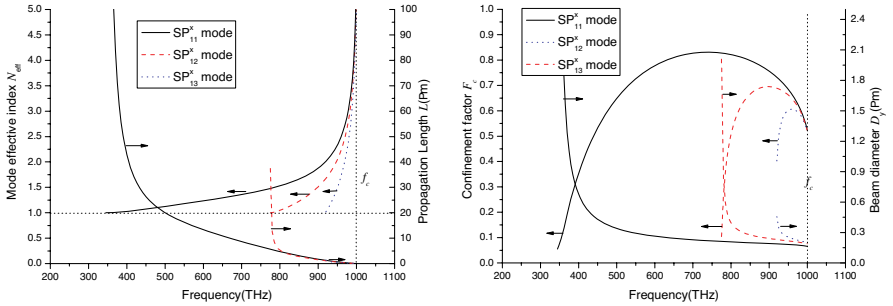

(a) Effective index and propagation lengths (b) Confinement factor and beam diameter

Figure 6. The propagation properties of the SPP modes in channel waveguide as a function of frequency.

Figure 7 shows the dependence of the propagation properties of SPP modes on the height of channel waveguide with $w = 50\,\text{nm}$ and $\lambda = 632.8\,\text{nm}$. It should be pointed out that cutoff heights for SPP modes exist in channel waveguides. The propagation lengths of SPP modes start to increase rapidly as the gap height decreasing towards the cutoff height. As the waveguide height increase, the confinement factor increases from 12% to 95%, and the propagation length approach $19\,\mu\text{m}$.

Figure 8 shows the distribution of magnetic field H_y for the SP_{11}^x

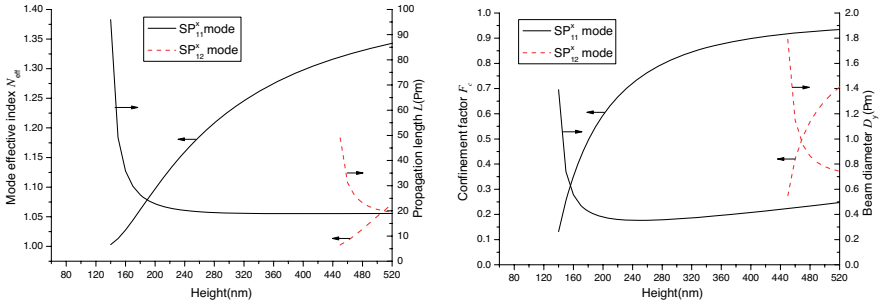

(a) Effective index and propagation length (b) Confinement factor and beam diameter

Figure 7. The propagation properties of the SPP mode in channel waveguide as a function of the height.

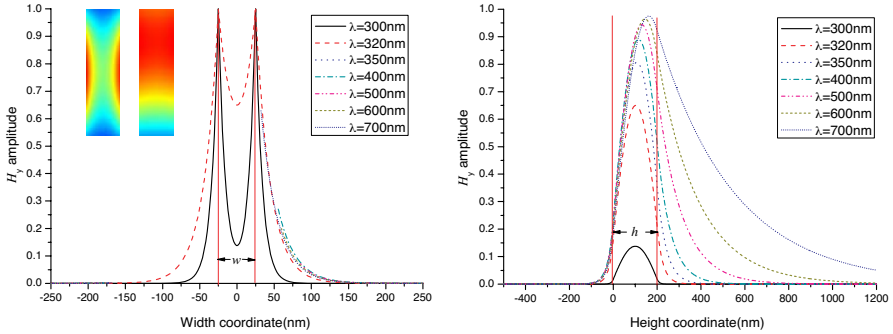

(a) H_y field distribution at y=h/2 (b) H_y field distribution at x=0

Figure 8. The distribution of magnetic field H_y for the fundamental mode SP_{11}^x in channel waveguide with $w = 50\,\text{nm}$ and $h = 200\,\text{nm}$. The inset shows the H_y field distributions in the air-core at $\lambda = 310\,\text{nm}$ and $632.8\,\text{nm}$ separately.

mode in a channel waveguide with $w = 50\,\text{nm}$ and $h = 200\,\text{nm}$. The discrepancy in the SPP guiding abilities between channel waveguide and gap waveguide is due to the difference in the field distribution in the air-core. While the field of SP_{11}^x mode at the bottom of gap waveguide remains to be a finite value, the field of SP_{11}^x mode in channel waveguide decreases to zero at the channel bottom due to the negative large permittivity of metal substrate. As the operation wavelength increases, the fields extend outward to the air-core and the confinement in the air-core of the channel waveguide decreases.

3.3. Rectangular-hole Waveguide

The extraordinary light transmission in subwavelength apertures has been investigated recently [36, 37]. It is shown that such apertures can support SPP modes, which can propagate even when the dimension of the aperture is smaller than the operation wavelength due to the red-shift of cutoff wavelengths of SPP modes. The rectangular-hole waveguide can be considered to be a special symmetric gap waveguide with silver substrate and silver cladding.

Figure 9 shows the propagation characteristics of the SPPs modes in the silver rectangular-hole waveguide with $w = 50\,\text{nm}$ and $h = 200\,\text{nm}$. As the operation frequency decreases, the SPP modes emerge from the slow wave region to the fast wave region before reaching cutoffs. In contrast to channel waveguide and gap waveguide, the SPP modes in the rectangular-hole waveguide have higher cutoff frequency, better confinement factors, and shorter propagation lengths. As the operation frequency decreases, the beam diameter along the y-direction slightly increase, but due to the simultaneous deceasing beam diameter along the x-direction, the confinement factors increase gradually. Moreover, the trade-off between the propagation length and the confinement factor for the cases of the gap and channel waveguides does not exist for the rectangular-hole waveguide. This interesting fact indicates that the SPP mode with better confinement in rectangular-hole waveguide can support relative longer distance propagation at some frequency. At the frequency of 585 THz, the propagation length is $8.5\,\mu\text{m}$ and the confinement factor is about 92%. In comparison with SP_{12}^x mode, the fundamental mode SP_{11}^x has longer propagation length, better confinement factor, and lower cutoff frequency.

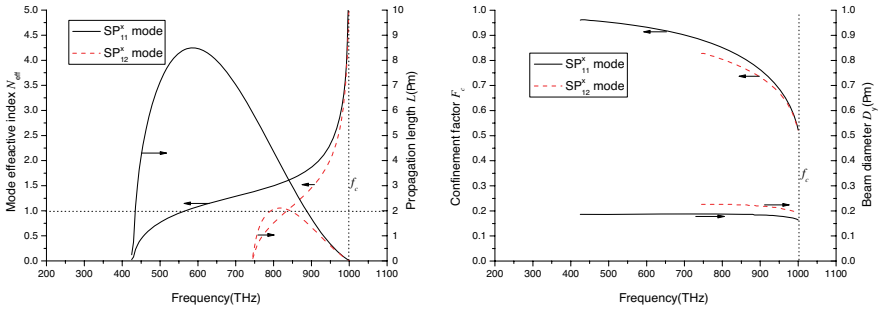

(a) Mode effective index and propagation length (b) Confinement factor and beam diameter

Figure 9. The propagation properties of the SPP modes in the rectangular-hole waveguide as a function of the frequency.

Figure 10 shows the dependency of propagation properties of the SPP modes on the height of rectangular-hole waveguide with $w = 50\,\text{nm}$ and $\lambda = 632.8\,\text{nm}$. It is shown that the cutoff height for the SP_{11}^x mode in the rectangular-hole waveguide is about 170 nm. At the cutoff height, the propagation length of the SPP mode approaches zero. As the waveguide height increases, the propagation length of the SP_{11}^x mode increases and the confinement factor remains about 95%.

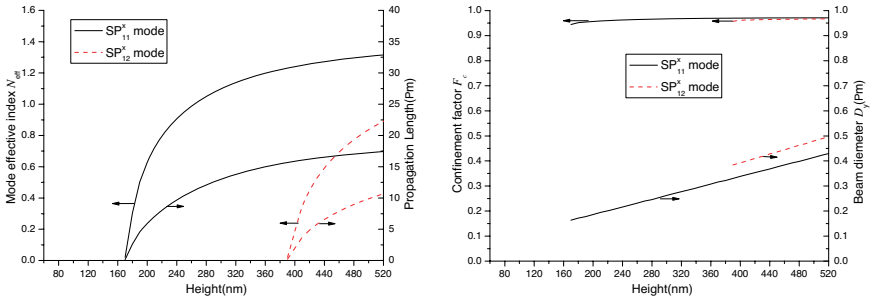

(a) Mode effective index and propagation length (b) Confinement factor and beam diameter

Figure 10. The propagation properties of the SPP modes in the rectangular-hole waveguide as a function of the height.

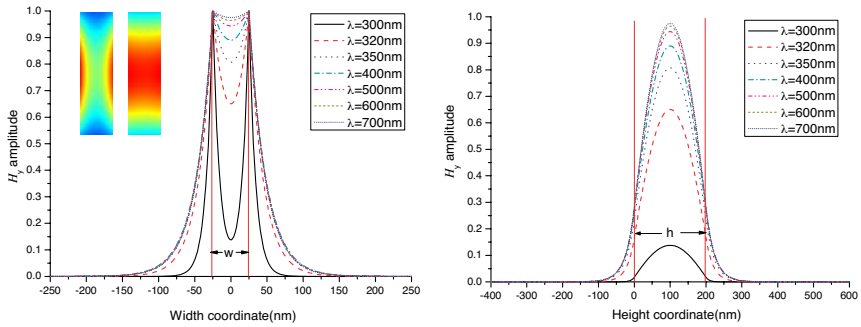

(a) H_y field distribution at $y=h/2$ (b) H_y field distribution at $x=0$

Figure 11. The distribution of magnetic field h_y for the fundamental mode in rectangular-hole waveguide with $w = 50\,\text{nm}$ and $h = 200\,\text{nm}$. The inset shows the H_y field distributions in the air-core at $\lambda = 310\,\text{nm}$ and 632.8 nm separately.

Figure 11 shows the distribution of magnetic field H_y for the SP_{11}^x mode in a rectangular hole waveguide with $w = 50\,\text{nm}$ and $h = 200\,\text{nm}$. Compared with gap waveguide and channel waveguide, the rectangular-hole waveguide shows better confinement in both transverse directions.

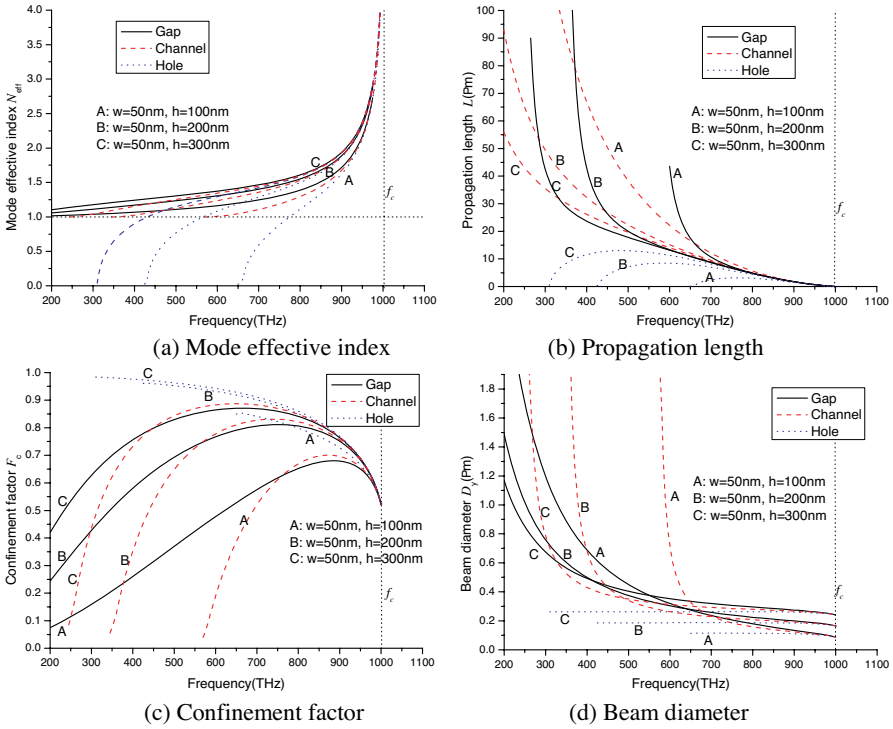

Figure 12. The propagation properties of the SP_{11}^x modes in the three metallic waveguides.

3.4. Comparison

In order to compare the propagation characteristics of the fundamental modes SP_{11}^x in gap, channel, and hole structures, three different size waveguides are analyzed from 200 THz to the critical frequency by using the complex effective dielectric constant method. Figure 12 shows the propagation properties of the fundamental mode as a function of the frequency. It shows that the propagation properties of the gap, channel, and rectangular-hole waveguides with the same size air-core is vary similar when the SP_{11}^x modes are close to the critical frequency, but their propagation properties diverge immensely as the operation frequency decreases. Among the three waveguides, the rectangular-hole waveguide has the best confinement factor and the shortest propagation length. The channel waveguide has shorter propagation length and better confinement than the gap waveguide when the mode is close to the critical frequency, but has longer propagation length and worse confinement factor when the mode is far

from the critical frequency. Moreover, it is important to note that the cutoff conditions in the channel and rectangular-hole waveguides are different, i.e., it is $\mathrm{Re}(\gamma_{cy}) = 0$ for the SPP modes in channel waveguide while it is $\mathrm{Re}(\beta) = 0$ for the SPP modes in gap waveguide. Thus, the propagation length of the SPP mode at cutoff in channel waveguide is very long while it is close to zero in the rectangular waveguide.

4. CONCLUSION

This paper introduces the application of complex effective dielectric constant method to analyze the metallic waveguides with rectangular-core. The effective index, propagation length, confinement factor, and beam diameter in three typical metallic waveguides are calculated from 200 THz to the critical frequency where the real part of metal permittivity is negative unity. The SPP modes in gap waveguide and channel waveguide are slow wave while the SPP modes in rectangular-hole waveguide can be fast wave or slow wave depending on the operation frequency. In comparison with the higher order mode, the fundamental mode has better confinement factor. It is found that cut-off frequency and cutoff height exist in channel waveguide and rectangular-hole waveguide. Because the cutoff conditions in the two waveguides are different, the channel and rectangular-hole waveguide behave different propagation properties at cutoffs. Among the three waveguides, the rectangular-hole waveguide has the best confinement factor and the shortest propagation length. Compared with the gap waveguide, the channel waveguide has shorter propagation length and better confinement when the operation frequency is near the critical frequency, but has longer propagation length and worst confinement when the operation frequency is far from the critical frequency. These results can provide some guideline in the design of nanoscale optical devices based on the dispersion characteristics of metallic waveguides.

ACKNOWLEDGMENT

This work is sponsored in part by the Office of Naval Research under Contract N00014-01-1-0713, the Department of the Air Force under Air Force Contract F19628-00-C- 0002, the Chinese National Foundation under Contract 60531020, Natural Science Foundation of Shandong Province under Contract Y2005G19, and The Chinese PSF under Grant No. 20060390331.

REFERENCES

1. Zayats, A. V., Smolyaninov, II, and A. A. Maradudin, "Nano-optics of surface plasmon polaritons," *Physics Reports*, Vol. 408, No. 3–4, 131–314, 2005.
2. Prasad, P. N., *Nanophotonics*, Wiley-Interscience, New Jersey, 2004.
3. Ozbay, E., "Plasmonics: merging photonics and electronics at manoscale dimensions," *Science*, Vol. 311, No. 5758, 189–193, 2006.
4. Chang, C. K., D. Z. Lin, C. S. Yeh, et al., "Experimental analysis of surface plasmon behavior in metallic circular slits," *Applied Physics Letters*, Vol. 90, No. 6, 2007.
5. Gordon, R., L. K. S. Kumar, and A. G. Brolo, "Resonant light transmission through a nanohole in a metal film," *IEEE Transactions on Nanotechnology*, Vol. 5, No. 3, 291–294, 2006.
6. Lin, L., R. J. Reeves, and R. J. Blaikie, "Surface-plasmon-enhanced light transmission through planar metallic films," *Physical Review B*, Vol. 74, No. 15, 2006.
7. Xiao, S., N. A. Mortensen, and M. Qiu, "Enhanced transmission through arrays of subwavelength holes in gold films coated by a finite dielectric layer," *Journal of the European Optical Society*, Vol. 2, No. 7, 2007.
8. Lin, L., R. J. Blaikie, and R. J. Reeves, "Surface-plasmon-enhanced optical transmission through planar metal films," *Journal of Electromagnetic Waves and Applications*, Vol. 19, No. 13, 1721–1728, 2005.
9. Bouhelier, A., J. Renger, M. R. Beversluis, et al., "Plasmon-coupled tip-enhanced near-field optical microscopy," *Journal of Microscopy*, Vol. 210, No. 3, 220–224, 2003.
10. Ditlbacher, H., J. R. Krenn, B. Lamprecht, et al., "Spectrally coded optical data storage by metal nanoparticles," *Opt. Lett*, Vol. 25, No. 8, 563–565, 2000.
11. Luo, X., "Surface plasmon resonant interference nanolithography technique," *Applied Physics Letters*, Vol. 84, No. 23, 4780–4782, 2004.
12. Prasad, P. N., *Introduction to Biophotonics*, Wiley-Interscience, New Jersey, 2003.
13. El-Kady, I., M. M. Sigalas, R. Biswas, et al., "Metallic photonic crystals at optical wavelengths," *Physical Review B*, Vol. 62, No. 23, 15299–15302, 2000.

14. Breukelaar, I., R. Charbonneau, and P. Berini, "Long-range surface plasmon-polariton mode cutoff and radiation," *Applied Physics Letters*, Vol. 88, No. 5, 051119, 2006.
15. Maier, S. A., "Observation of coupled plasmon-polariton modes in Au nanoparticle chain waveguides of different lengths: Estimation of waveguide loss," *Applied Physics Letters*, Vol. 81, No. 9, 1714, 2002.
16. Liaw, J. W., M. K. Kuo, and C. N. Liao, "Plasmon resonances of spherical and ellipsoidal nanoparticles," *Journal of Electromagnetic Waves and Applications*, Vol. 19, No. 13, 1787–1794, 2005.
17. Imura, K., T. Nagahara, and H. Okamoto, "Near-field optical imaging of plasmon modes in gold nanorods," *Journal of Chemical Physics*, Vol. 122, No. 15, 154701, 2005.
18. Seidel, J., "Surface plasmon transmission across narrow grooves in thin silver films," *Applied Physics Letters*, Vol. 82, No. 9, 1368, 2003.
19. Pile, D. F. P. and D. K. Gramotnev, "Channel plasmon-polariton in a triangular groove on a metal surface," *Optics Letters*, Vol. 29, No. 10, 1069–1071, 2004.
20. Bozhevolnyi, S. I., V. S. Volkov, E. Devaux, et al., "Channel plasmon-polariton guiding by subwavelength metal grooves," *Physical Review Letters*, Vol. 95, No. 4, 46802, 2005.
21. Sarid, D., "Long-range surface-plasma waves on very thin metal films," *Physical Review Letters*, Vol. 47, No. 26, 1927–1930, 1981.
22. Kuwamura, Y., M. Fukui, and O. Tada, "Experimental observation of long-range surface plasmon polaritons," *Journal of the Physical Society of Japan*, Vol. 52, No. 7, 2350–2355, 1983.
23. Guo, J. and R. Adato, "Extended long range plasmon waves in finite thickness metal film and layered dielectric materials," *Optics Express*, Vol. 14, No. 25, 12409–12418, 2006.
24. Pile, D. F. P., T. Ogawa, D. K. Gramotnev, et al., "Two-dimensionally localized modes of a nanoscale gap plasmon waveguide," *Applied Physics Letters*, Vol. 87, No. 26, 261114, 2005.
25. Liu, L., Z. Han, and S. He, "Novel surface plasmon waveguide for high integration," *Optics Express*, Vol. 13, No. 17, 6645–6650, 2005.
26. Satuby, Y. and M. Orenstein, "Surface-plasmon-polariton modes in deep metallic trenches — measurement and analysis," *Optics Express*, Vol. 15, No. 7, 4247–4252, 2007.

27. Bozhevolnyi, S. I., V. S. Volkov, E. Devaux, et al., "Channel plasmon subwavelength waveguide components including interferometers and ring resonators," *Nature*, Vol. 440, No. 7083, 508–511, 2006.
28. Collin, S., F. Pardo, and J. L. Pelouard, "Waveguiding in nanoscale metallic apertures," *Optics Express*, Vol. 15, No. 7, 4310–4320, 2007.
29. Saj, W., "FDTD simulations of 2D plasmon waveguide on silver nanorods in hexagonal lattice," *Optics Express*, Vol. 13, No. 13, 4818–4827, 2005.
30. Jin, E. X. and X. Xu, "Finitte-difference time-domain studies on optical transmission through planar nano-apertures in a metal film," *Japanese Journal of Applied Physics*, Vol. 43, No. 1, 407–417, 2004.
31. Kawano, K. and T. Kitoh, *Introduction to Optical Waveguide Analysis*, Wiley, Chichester, 2001.
32. Bozhevolnyi, S. I., "Effective-index modeling of channel plasmon polaritons," *Optics Express*, Vol. 14, No. 20, 9467–9476, 2006.
33. Wu, B. I., T. M. Grzegorczyk, Y. Zhang, et al., "Guided modes with imaginary transverse wave number in a slab waveguide with negative permittivity and permeability," *Journal of Applied Physics*, Vol. 93, No. 11, 9386, 2003.
34. Sönnichsen, C., "Plasmons in metal nanostructures," Ph.D. thesis, Ludwig Maximilians Universität, München, 2001.
35. Veronis, G. and S. Fan, "Bends and splitters in metal-dielectric-metal subwavelength plasmonic waveguides," *Applied Physics Letters*, Vol. 87, No. 13, 131102, 2005.
36. Bai, M. and N. Garcia, "Transmission of light by a single subwavelength cylindrical hole in metallic films," *Applied Physics Letters*, Vol. 89, No. 14, 2006.
37. Kim, K. Y., Y. K. Cho, H. S. Tae, et al., "Optical guided dispersions and subwavelength transmissions in dispersive plasmonic circular holes," *Opto-Electronics Review*, Vol. 14, No. 3, 233–241, 2006.